



**HAL**  
open science

# Sub-10 nm spatial resolution for electrical properties measurements using bimodal excitation in electric force microscopy

Khaled Kaja, Denis Mariolle, Nicolas Chevalier, Adnan Naja, Mustapha Jouiad

## ► To cite this version:

Khaled Kaja, Denis Mariolle, Nicolas Chevalier, Adnan Naja, Mustapha Jouiad. Sub-10 nm spatial resolution for electrical properties measurements using bimodal excitation in electric force microscopy. *Review of Scientific Instruments*, 2021, 92 (2), 10.1063/5.0038335 . hal-03627683

**HAL Id: hal-03627683**

**<https://u-picardie.hal.science/hal-03627683v1>**








Submitted on 26 Sep 2024

**HAL** is a multi-disciplinary open access archive for the deposit and dissemination of scientific research documents, whether they are published or not. The documents may come from teaching and research institutions in France or abroad, or from public or private research centers.

L'archive ouverte pluridisciplinaire **HAL**, est destinée au dépôt et à la diffusion de documents scientifiques de niveau recherche, publiés ou non, émanant des établissements d'enseignement et de recherche français ou étrangers, des laboratoires publics ou privés.

RESEARCH ARTICLE | FEBRUARY 12 2021

# Sub-10 nm spatial resolution for electrical properties measurements using bimodal excitation in electric force microscopy

Khaled Kaja   ; Denis Mariolle  ; Nicolas Chevalier  ; Adnan Naja  ; Mustapha Jouiad  

 Check for updates

*Rev. Sci. Instrum.* 92, 023703 (2021)

<https://doi.org/10.1063/5.0038335>



## Articles You May Be Interested In

Erratum: "Sub-10 nm spatial resolution for electrical properties measurements using bimodal excitation in electric force microscopy" [*Rev. Sci. Instrum.* 92, 023703 (2021)]

*Rev Sci Instrum* (April 2021)

Quantification of van der Waals forces in bimodal and trimodal AFM

*J. Chem. Phys.* (May 2023)

Enhanced sensitivity and contrast with bimodal atomic force microscopy with small and ultra-small amplitudes in ambient conditions

*Appl. Phys. Lett.* (December 2013)

26 September 2024 14:03:55

Nanotechnology & Materials Science


Optics & Photonics

Impedance Analysis

Scanning Probe Microscopy

Sensors


Failure Analysis & Semiconductors



**Unlock the Full Spectrum.**  
From DC to 8.5 GHz.

Your Application. Measured.

[Find out more](#)



# Sub-10 nm spatial resolution for electrical properties measurements using bimodal excitation in electric force microscopy

Cite as: *Rev. Sci. Instrum.* **92**, 023703 (2021); doi: [10.1063/5.0038335](https://doi.org/10.1063/5.0038335)

Submitted: 20 November 2020 • Accepted: 13 January 2021 •

Published Online: 12 February 2021



View Online



Export Citation



CrossMark

Khaled Kaja,<sup>1,2,3,a)</sup>  Denis Mariolle,<sup>4</sup>  Nicolas Chevalier,<sup>4</sup>  Adnan Naja,<sup>2</sup>  and Mustapha Jouiad<sup>5,a)</sup> 

## AFFILIATIONS

<sup>1</sup>Laboratoire National de Métrologie et d'Essais, 29 Rue Roger Hennequin, 78190 Trappes, France

<sup>2</sup>Laboratory of Physics and Modelling, EDST, Lebanese University, 1300 Tripoli, Lebanon

<sup>3</sup>Department of General Sciences, Prince Sultan University, 11586 Riyadh, Saudi Arabia

<sup>4</sup>Univ. Grenoble Alpes, CEA, Leti, F-38000 Grenoble, France

<sup>5</sup>Laboratory of Physics of Condensed Matter, LPMC, Université de Picardie Jules Verne, 80093 Amiens, France

<sup>a)</sup> Authors to whom correspondence should be addressed: [khaled.kaja@lne.fr](mailto:khaled.kaja@lne.fr)  
and [mustapha.jouiad@u-picardie.fr](mailto:mustapha.jouiad@u-picardie.fr)

## ABSTRACT

We demonstrate that under ambient and humidity-controlled conditions, operation of bimodal excitation single-scan electric force microscopy with no electrical feedback loop increases the spatial resolution of surface electrical property measurements down to the 5 nm limit. This technical improvement is featured on epitaxial graphene layers on SiC, which is used as a model sample. The experimental conditions developed to achieve such resolution are discussed and linked to the stable imaging achieved using the proposed method. The application of the herein reported method is achieved without the need to apply DC bias voltages, which benefits specimens that are highly sensitive to polarization. Besides, it allows the simultaneous parallel acquisition of surface electrical properties (such as contact potential difference) at the same scanning rate as in amplitude modulation atomic force microscopy (AFM) topography measurements. This makes it attractive for applications in high scanning speed AFM experiments in various fields for material screening and metrology of semiconductor systems.

Published under license by AIP Publishing. <https://doi.org/10.1063/5.0038335>

## I. INTRODUCTION

A new paradigm in nano-scale device fabrication has been introduced with the first isolation of graphene in 2004.<sup>1,2</sup> Two-dimensional crystals have become the building blocks of novel nanostructures for a virtually unlimited spectrum of technological applications.<sup>3–5</sup> The nano-characterization and nano-metrology by atomic force microscopy (AFM) of this new class of materials require ultra-high-resolution methods and ultra-fast imaging techniques. A strong focus is made on measuring the electrical and electrostatic properties of surfaces at the nanoscale as they constitute one of the fundamental functionalities of most nano-fabricated structures.

In an AFM setup, electrostatic forces would build between the probe and the sample surface whenever an electric field is present

between them, which could stem from different origins such as work function differences, surface potential variations, and the presence of charges or dipoles. Interplay between van der Waals and electrostatic forces is highly dependent on the separation distance between the AFM tip and the sample surface.<sup>6–8</sup> It is well known that the spatial resolution of electrical AFM measurements is strongly dependent on the capacitive contributions of the geometrical parts of the probe. These include the contribution of the spherical tip apex, a trunked cone, and the cantilever.<sup>6,9,10</sup> Since these parts have largely different dimensions, they form parallel capacitances with the sample surface, having different weights depending directly on the corresponding separation distances.<sup>11,12</sup> Additionally, the capacitive contributions of the probe's geometry are strongly altered by the nature of the electrical signal probed. Studies showed that probing the electrical force in a closed-loop scheme [corresponding modes are

identified as amplitude modulation (AM) methods] exhibits a stronger contribution from the very large cantilever and cone compared to the spherical tip apex. This leads to a large averaging of the probed signal resulting in low spatial resolutions.<sup>12,13</sup> It also reduces the accuracy of the electric measurements, more specifically the contact potential difference (CPD) measured in the so-called Kelvin probe force microscopy (KPFM) method. However, when the gradient of the electric force is measured [corresponding modes are identified as frequency modulation (FM) methods], the contributions of the cantilever and cone are reduced, which improves the accuracy of the measured contact potential difference and enhances the spatial resolution.<sup>13–16</sup> Several works argue that the measurements in FM KPFM tend to provide quantifiable values of the contact potential difference compared to other techniques.<sup>15,17</sup> Nevertheless, AM KPFM modes are usually easier to implement and use on most commercially available AFM systems.

## II. THEORY

In fact, the KPFM method probes the changes in electrostatic forces between the tip and the sample, which allows for the measurement of local variations in the work function difference between the tip and the sample. Since the work function is an extreme surface dependent property, KPFM has demonstrated its advantageous use in a wide spectrum of applications in semiconductors,<sup>18–21</sup> corruptions,<sup>22,23</sup> 2D materials and thin films,<sup>24–28</sup> polymers,<sup>29–31</sup> and biological studies.<sup>32</sup>

The KPFM method is commonly applied in conjunction with topography measurement in AFM with or without simultaneous additional methods such as nano-mechanical mapping.<sup>33</sup> The AFM tip is, therefore, prone to a multitude of interaction fields with the sample, highly dependent on their mutual separation distance. In the absence of magnetic fields, the most prominent long-range interactions taking place between the tip and the sample in AFM are van der Waals and electrostatic forces. The distance dependencies of these two interactions between the tip and the sample in AFM have been extensively studied in the literature.<sup>9,10</sup>

To specifically probe the electrostatic interaction, external bias voltages are applied between the tip and the sample, which act as a small capacitor system with a rather complicated geometry. The electrostatic potential energy of the tip–sample system is also modulated to enable its separation from other interaction contributions using lock-in amplifier techniques. The resulting tip–sample potential difference  $V_{ts}$  is given by

$$V_{ts} = V_{tip} - V_{sample} = (V_{cpd} \pm V_{dc}) + V_{ac} \sin(\omega_{el}t).$$

The contact potential difference  $V_{cpd}$  builds up naturally between the tip and the sample, when electrically connected, due to the differences in their respective work functions such that  $|V_{cpd}| = \frac{|\phi_{tip} - \phi_{sample}|}{e}$ .  $V_{dc}$  is an adjustable DC bias voltage applied to the tip or the sample depending on the experimental polarization setup (e.g., [supplementary material](#)).  $V_{ac} \sin(\omega_{el}t)$  is the alternating voltage applied to the system to modulate the electrostatic interaction at the frequency  $f_{el} = \frac{\omega_{el}}{2\pi}$ . The electrostatic force can be measured in KPFM between the tip and the sample by  $F_{el} = \frac{1}{2} \frac{\partial C}{\partial z} V_{ts}^2$ .

Nevertheless, a general description of the force between the tip and the sample encompasses the presence of charges on the sample surface.<sup>34</sup> This adds a Coulomb interaction component to the electrostatic force expression given by  $\frac{q_s q_t}{4\pi\epsilon_0 z^2}$ , where  $q_s$  represents superficial surface charges and  $q_t$  represents the total charge on the point conductive probe.

Taking all these elements into account, the electrostatic force has, therefore, three spectral components given by

$$F_{dc} = \frac{1}{2} \frac{\partial C}{\partial z} (V_{cpd} - V_{dc})^2 + \frac{1}{4} \frac{\partial C}{\partial z} V_{ac}^2 + \frac{q_s q_t}{4\pi\epsilon_0 z^2} (V_{cpd} - V_{dc}), \quad (1)$$

$$F_{\omega_{el}} = \left[ \frac{\partial C}{\partial z} (V_{cpd} - V_{dc}) + \frac{q_s q_t}{4\pi\epsilon_0 z^2} \right] V_{ac} \sin(\omega_{el}t), \quad (2)$$

$$F_{2\omega_{el}} = -\frac{1}{4} \frac{\partial C}{\partial z} V_{ac}^2 \cos(2\omega_{el}t). \quad (3)$$

Closed-loop AM KPFM methods measure the amplitude of the  $F_{\omega_{el}}$  component and feed it to a Kelvin controller. The latter adjusts the value of the DC bias voltage such that  $V_{dc} = V_{cpd}$ , which minimizes (ideally nullifies) the amplitude of the electrically driven vibrations. Closed-loop AM KPFM methods are the most commonly used ones on commercial AFM systems. These methods are generally considered to provide “semi-quantifiable” maps of the contact potential difference of the sample. In fact, although local relative variations in the surface contact potential difference could be quantified, the absolute measured values remain highly controversial. Nonetheless, it has also been shown that closed-loop methods suffer from several artifact sources related to the experimental parameters of the KPFM setup and the feedback system.<sup>35</sup>

The open-loop KPFM methods, however, require no Kelvin controller feedback as they directly measure the amplitude of the force  $F_{\omega_{el}}$ . Usually the DC bias in these methods is set to zero. By doing so, the open-loop KPFM methods benefit from artifact-free measurements and from scanning rates unobstructed by the bandwidth of the Kelvin controller. This makes their use highly attractive for fast-scanning nano-metrological applications.

In this work, we combine the ease of use of amplitude modulation methods with the benefits of open-loop schemes (with no feedback) to exploit the distance dependencies of the capacitive contributions and propose an electric force microscopy method capable of achieving a 5 nm spatial resolution under controlled environment. Our method is based on a single-scan measurement using a bimodal excitation of the cantilever. We call it bimodal single-scan electric force microscopy (BM SS-EFM).

## III. MATERIAL AND METHODS

### A. BM SS-EFM setup

Experiments are carried out on a Dimension 3100 AFM equipped with a Nanoscope IIIa controller and Quadrex electronics (Veeco, USA). A rectangular cantilever ( $k = 3 \text{ N m}^{-1}$ ) with a PtIr-coated AFM tip (Nanosensors) is used. The first two eigenfrequencies of the cantilever are, respectively, measured at  $f_0 \approx 65 \text{ kHz}$  and  $f_1 \approx 392 \text{ kHz}$ . Our BM SS-EFM method consists of a single



scan bimodal mode during which the electrostatic force is measured simultaneously with the surface topography in the amplitude modulation (AM-AFM) mode. During the scanning procedure, the surface topography is acquired at  $f_0$  using the internal feedback loop of the Nanscope IIIa system. An external signal generator (HP33120A) is used to apply simultaneously the electrical modulation  $V_{ac} \sin(\omega_{el}t)$  at a frequency  $f_1$  of the second eigenmode. This signal is directly connected to the cantilever via a Signal Access Module (SAM) box connected to the microscope. The cantilever deflection signal is acquired in parallel using a homemade derivation card and then fed to an external lock-in amplifier (Signal Recovery DSP 7280) locked at frequency  $f_1$  to extract the amplitude  $A_1 = \sqrt{x_1^2 + y_1^2}$  and the phase  $\varphi_1 = \arctan(x_1/y_1)$ . The “in-phase” component  $x_1$  and the “quadrature” component  $y_1$ , representing the electrical oscillation signal as a vector relative to the lock-in reference oscillator, were preferred as output signals to preserve the sign of the contact potential difference  $V_{cpd}$ . The DC bias voltage in BM SS-EFM is set to zero ( $V_{dc} = 0$ ) and the sample is grounded.

## B. Sample description

The sample consists of epitaxial graphene layers thermally grown on *n*-doped, Si-terminated, 6H-SiC(0001) substrate as described elsewhere.<sup>25,36</sup> The SiC substrate is initially annealed at 2000 °C for 30 min in an Ar environment under 600 mbar pressure. Raman spectroscopy and micro-Raman imaging were used to identify the formation of graphene layers, of different thicknesses, on the sample surface.<sup>37</sup> Earlier, we have shown that the surface potential of graphene flakes on 6H-SiC(0001) surface is highly dependent on the number of graphene layers.<sup>25,36</sup> A correlation between closed-loop AM KPFM measurements and x-ray photoemission electron microscopy (XPEEM) has been carried out<sup>25</sup> on the exact same sample used in this work. Results show that the work function of graphene in this case increases with the number of layers ranging from  $\sim 4.32 \pm 0.03$  eV for one-layer graphene up to  $\sim 4.59 \pm 0.07$  eV for multilayer-graphene (five layers). A difference of about  $\sim 0.11$  eV was also measured between the bare SiC substrate and the first graphene layer. A charge transfer occurring through a buffer layer between the SiC substrate and graphene has been reported at the origin of the work function variations. The charge transfer is independent of the number of graphene layers, which leads to a screening effect on the surface potential as the thickness of layers increases. Hence, the potential dependent contrast observed on the samples used in KPFM measurements of this study is directly related to the changes in the work function of the graphene layers formed on the surface, depending on their thickness.<sup>25,36</sup> Similar results have been reported in the literature.<sup>24,38</sup> The sample was chosen to demonstrate the lateral resolution enhancement of the BM SS-EFM method presented here because the domains corresponding to graphene flakes have pronounced surface potential differences easily measured in KPFM.

## IV. RESULTS

Only BM SS-EFM will be considered in regard of the enhancement in the spatial resolution of electrical measurements under ambient temperature and humidity-controlled environment. The

experimental limits and conditions of the stable imaging in BM SS-EFM for both surface topography in AM-AFM and simultaneous electrical property mapping will be discussed.

## A. The spatial resolution

The spatial resolution is generally described as the power of an imaging system to differentiate between two features separated by a certain distance. The smaller the distance between the features captured by the imaging system is, the higher is the spatial resolution of the system if it could resolve them separately with minimal convolutions.<sup>39–41</sup> Here, the spatial resolution of the electrical AFM measurements is determined using line profiles across an edge step between two regions of high variation in contact potential difference. The quantification of the spatial resolution is given by the width of the transition zone at the edge where the electrical signal changes from 16% to 84% of its value.<sup>41</sup> Other authors calculated the spatial resolution of electrical AFM imaging using variations across edges with the 25%–75%<sup>11,12,42</sup> and 10%–90% limits.<sup>17</sup> This approach to evaluate spatial resolution is the best-suited method for analytical instruments and surface measurement techniques.<sup>40</sup>

## B. The improvement of spatial resolution

To highlight the enhancement in the spatial resolution achievable in this study, imaging results acquired in the same region of the sample by closed-loop lift mode KPFM and BM SS-EFM were compared. We chose to make a comparison of the imaging results between these two methods since lift-mode KPFM has been shown to provide a correlation between the contact potential difference and the number of graphene layer on our sample. More details are described in Sec. III. In the lift mode KPFM measurements, the surface topography is acquired in a first line scan using the AM-AFM method. The cantilever is mechanically driven at its first eigenmode frequency  $f_0$ , while the feedback system maintains constant mechanical vibration set point amplitude  $A_{sp} \sim 35$  nm (around 70% of the free oscillations amplitude). In a second scan along the same line, the tip is lifted upward by a so-called “lift height” distance LH (here LH = 20 nm). In this second scan, the mechanical driving signal is cut off, and the cantilever is driven to oscillations by means of a sinusoidal electrical signal  $V_{ac} \sin(\omega_{el}t)$ . The tip redraws the surface topography of the line acquired in the first scan. The frequency of the electrically driven oscillations of the cantilever is set in this case to the first eigenmode frequency  $f_0$ , same as for the first topography scan. As previously described for closed-loop AM KPFM, a Kelvin controller feedback system adjusts a static bias voltage  $V_{dc}$  to minimize (ideally nullify) the amplitude of the electrically driven oscillations.

Figures 1(a) and 1(b) show the surface topography of the SiC sample and the map of the contact potential difference variations, respectively. Results show no crosstalk between the two imaging channels. As stated in Sec. III, the variations in the contact potential difference at the surface of this sample have been shown to be directly associated with the thickness of the graphene layer coverage over the SiC substrate.<sup>25,36</sup>

BM SS-EFM mode measurements were conducted on the same area of the sample surface. The method consists of a single scan mode during which the cantilever is driven to oscillations both

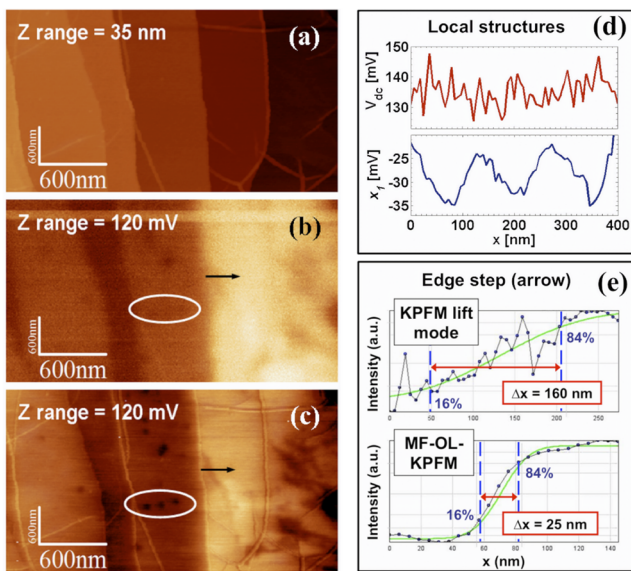


**FIG. 1.** (a) Topography map of epitaxial graphene layers on the SiC substrate obtained in AM-AFM mode. (b) Corresponding contact potential difference map obtained in lift-mode KFM at a lift height  $LH = 20$  nm. (c) Map of the  $x_1$  channel revealing the variations in the electrostatic force obtained in BM SS-EFM. (d) Cross section profiles across structures highlighted by the white ellipse on the images showing the power of resolution in BM SS-EFM compared to lift-mode KPFM. (e) Evaluation of the spatial resolution of each method over a step variation in contact potential difference contrast.

mechanically and electrically. Mechanical oscillations are driven by the dither piezo at the frequency of the first eigenmode  $f_0 = 65$  kHz. Simultaneously, an electrical driving signal  $V_{ac} \sin(\omega_{el} t)$  is directly applied to the cantilever at the second eigenmode frequency  $f_1 = 392$  kHz. It is worth noting that the amplitude of the electrical driving signal in BM SS-EFM is set equal to the electrical signal in the lift-mode KPFM measurement, i.e.,  $V_{ac} = 2$  V. The surface topography is normally acquired in AM-AFM mode by maintaining a constant amplitude of mechanical oscillations at the set point value  $A_{sp} \sim 35$  nm (same as for the lift-mode measurements). Simultaneously, we capture the fast demodulation mode's outputs ( $x_1$  and  $y_1$ ) of an external lock-in amplifier set at the second eigenmode frequency  $f_1$ . The images of the  $x_1$  and  $y_1$  signals were recorded by using auxiliary entries in the commercial microscope software. The amplitudes of the free oscillations of the cantilever at the two eigenmodes [ $A_0^{(0)}$  at  $f_0$  and  $A_1^{(0)}$  at  $f_1$ ] were calibrated separately such that  $A_1^{(0)}/A_0^{(0)} = 0.13$ . The choice of this particular ratio is discussed in detail in Sec. V C 2. Figure 1(c) shows the map of the  $x_1$  signal at the output of the lock-in amplifier of the BM SS-EFM setup. In fact, the phase signal of the lock-in amplifier is adjusted so that the magnitude of the signal is mostly in the  $x_1$  output. The map of the  $x_1$  channel shows an identical trend of contrast compared to the contact potential difference map obtained in lift-mode KPFM in Fig. 1(b). This supports the fact that this signal corresponds to the electrostatic force  $F_{\omega_{el}}$  [see Eq. (2)], and it is directly proportional to the variation of the contact potential difference

on the sample, which is linked to the variations in the graphene layer thickness. Nevertheless, the enhancement in the spatial resolution of the BM SS-EFM image is visually clear. For comparison, Fig. 1(d) shows the cross section profiles recorded across specific features on the sample (highlighted by the white elliptical shape). The results clearly show that the BM SS-EFM imaging is capable of resolving the three features along the 400 nm line, which are completely undistinguishable on the lift-mode KPFM image [Fig. 1(b)]. To quantify this increase in the spatial resolution, we compare two cross section lines recorded along a step of electrical property variation marked with the black arrow on the images. It is worth noting that we have intentionally selected this particular step, which is only observed on the surface potential images, Figs. 1(b) and 1(c), away from the topography step edge on the SiC substrate. This is with the aim to avoid any convolution of our comparison with the resolution of the topography measurements. Figure 1(e) shows the two cross section profiles from lift-mode KPFM and BM SS-EFM fitted with an edge step function using the ImageJ® software. A width  $\Delta x = 160$  nm of the 16%–84% transition region at the step is measured in the case of lift-mode KPFM measurements. The BM SS-EFM results demonstrate a sixfold increase in spatial resolution under ambient conditions, with a width of the transition region  $\Delta x = 28$  nm.

This improvement is attributed to several factors that will be discussed in Sec. V. Ding *et al.*<sup>43</sup> showed a spatial resolution  $\sim 15$  nm under ambient conditions using a multi-frequency scheme in conjunction with the lift-mode KPFM. Nevertheless, their estimation is made over a topographically varying edge, which renders the evaluation of the spatial resolution in electrical measurement a little bit more complex. Zerweck *et al.*<sup>17</sup> demonstrated a spatial resolution in the order of 50 nm measured in frequency modulation FM-KPFM, under vacuum conditions, over step edges between KCl and Au using usual AFM probes. Using super sharp AFM probes coated with a very thin layer of chromium, these authors showed a spatial resolution of about 10 nm under ultra-high-vacuum (UHV) conditions. Sommerhalter *et al.*<sup>44</sup> also reported a spatial resolution of  $\sim 20$  nm for AM-KPFM measurements in UHV using the electrical oscillation at the second eigenmode of the cantilever. These reported values show that the spatial resolution that we demonstrate in this work under ambient conditions using BM SS-EFM is comparable to the results obtained under UHV conditions. This constitutes a strong advantage of our method since it allows reaching these resolution values without the need to use expensive UHV setups. It also allows the characterization of sensitive samples (biological and organic), which might be hindered under the UHV environment.

### C. Humidity reduced environment: Enhanced local resolution

Although our results show an important enhancement in the spatial resolution of contact potential difference dependent measurements under ambient conditions, it is well known that the ambient humidity has a considerable effect on the sharpness of the contrast in AFM electrical measurements.<sup>45,46</sup> We have, therefore, investigated experimentally the effect of a reduced humidity environment on the quality of the spatial resolution of our BM SS-EFM measurements. To this end, the AFM microscope is placed inside

a homemade Plexiglas cabinet fitted with a small airlock chamber and a glove box system. Using a continuous flow of nitrogen inside the cabinet, the relative humidity level is monitored with a miniaturized sensor placed at the proximity of the sample holder. Prior to measurements, the sample was heated at 150 °C for about 2 h and then transferred to the airlock chamber of the cabinet under nitrogen flow. The system was kept to settle under a relative humidity level  $RH\% \sim 2 \pm 0.2\%$  for an hour prior to scanning. The main goal of the sample heating is to dissipate and clean surface contamination and accelerate the water molecule removal from the surface assisted by the flow of nitrogen gas.

A comparison between imaging results in lift-mode KPFM and BM SS-EFM is conducted under reduced humidity conditions, similar to that performed in ambient. Figure 2(a) shows a 1  $\mu\text{m}$  scan obtained in AM-AFM mode of the SiC surface topography covered with graphene. Figures 2(b) and 2(c) show the map of the contact potential difference obtained in lift-mode KPFM and the  $x_1$  channel in BM SS-EFM, respectively. The experimental conditions for both modes are exactly the same as for the measurements made in Fig. 1, in terms of oscillation amplitudes, frequencies, and lift height. While lift-mode KPFM imaging (obtained at ambient humidity level  $RH\% \sim 25\%$ ) renders a very blurry contrast, the BM SS-EFM results (obtained at  $\sim 2\%$  relative humidity) reveal a greater improvement in the spatial resolution measured on the cross section profile in Fig. 2(d) at  $\Delta x \sim 5$  nm. Both measurements present the same trend in electrical contrast, indicating again that the map of the BM SS-EFM here is directly dependent on the variations in the work function of graphene layers. This again correlates very well with the measurements that we have previously reported in Ref. 25 using XPEEM

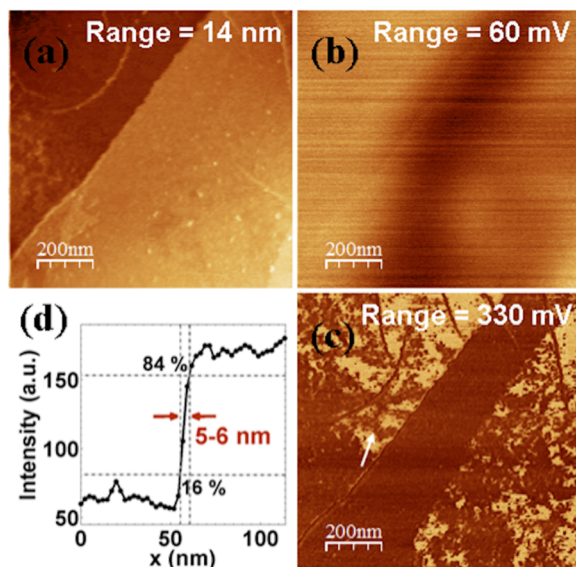


**FIG. 2.** (a) Topography map of a 1  $\mu\text{m}^2$  area showing three regions of the SiC substrate covered with graphene layers. (b) Contact potential difference map measured in lift-mode KPFM at  $LH = 20$  nm and  $RH\% \sim 25\%$ , showing very blurry contrast. (c) Map of the  $x_1$  signal recorded in BM SS-EFM at  $RH\% \sim 2\%$ , showing a very sharp contrast and spatial resolution of  $\sim 5$  nm estimated from the cross section profile (d).

characterization on the exact same sample.<sup>36</sup> The very-high resolution images obtained in BM SS-EFM in a reduced humidity environment reveal the nanostructure of the epitaxial growth of graphene layers on SiC. This result shows the coverage of graphene on the SiC steps and gives a greater insight into its quality.

The improvement in spatial resolution achieved in this work offers important means to study potential dependent surface structures *in situ* at high scanning rates. This is mainly due to the fact that measurements in BM SS-EFM are not constrained by the bandwidth of a Kelvin controller and can be achieved at the same scanning rates as in AM-AFM. The spatial resolution reported in this work under reduced humidity is about two-orders of magnitude better than conventional lift-mode KPFM measurements under ambient conditions. It also competes with the 10 nm resolution values reported in the literature in UHV using very sharp AFM probes, which usually have a very fragile apex and are relatively expensive.

## V. DISCUSSION

We attribute the enhancement in the spatial resolution achieved in this work to two main factors: (i) the relative contributions of the probe's geometrical elements related to the distance between the tip and the sample as well as to the bimodal shape of the cantilever and (ii) the interaction of the surface water layers with graphene, controlled by reducing the relative humidity of the measurement environment.

### A. Probe geometry and cantilever shape

In order to compare the relative contributions of the spherical apex, cone, and cantilever to the total signal measured both in lift-mode KPFM and in BM SS-EFM, we used the model proposed by Hudlet *et al.*<sup>9</sup> to calculate the first derivative of the capacitances between the probe and the sample. In Fig. 3, we show the relative contributions of each probe element for a tip to sample separation distance up to 300 nm.

In BM SS-EFM, the cantilever has a bimodal shape vibrating simultaneously at the first and second eigenmodes as presented by the bold black line in the inset of Fig. 3(a). To calculate this shape, we have taken into account the relative ratio between the amplitudes of vibrations  $A_1^{(0)}/A_0^{(0)} = 0.13$ . The distance between the tip and the sample in this case is thus given by  $z = D - (H + A_0 + A_1)$ , where  $D$  is the mean equilibrium distance in AM-AFM and  $H$  is the height of the cone. We note that the dashed blue line in the inset corresponds to the shape of the first eigenmode plotted for visual guidance. The plots in Fig. 3(a) indicate that for distance  $z \leq 12$  nm, the spherical tip apex dominates (larger than 40%) the electrostatic force between the tip and the sample. Therefore, with the smaller distance between the tip and the sample surface in BM SS-EFM mode, the enhanced spatial resolution obtained experimentally under ambient conditions is clearly related to the concentrated signal at the spherical tip apex. Girard and Titkov<sup>13</sup> and Dunaevskiy *et al.*<sup>14</sup> suggested an analytical expression to estimate the spatial resolution of electrical AFM measurements considering only the tip apex capacitance. They considered it as the diameter of a disc area under the tip  $D_{area} \propto a\sqrt{Rz}$ , where the term  $a$  depends on the nature of the probed signal (i.e., force or force gradient). Using the experimental parameters in our BM SS-EFM measurements for  $R = 20$  nm and for  $z = 30$  nm, the



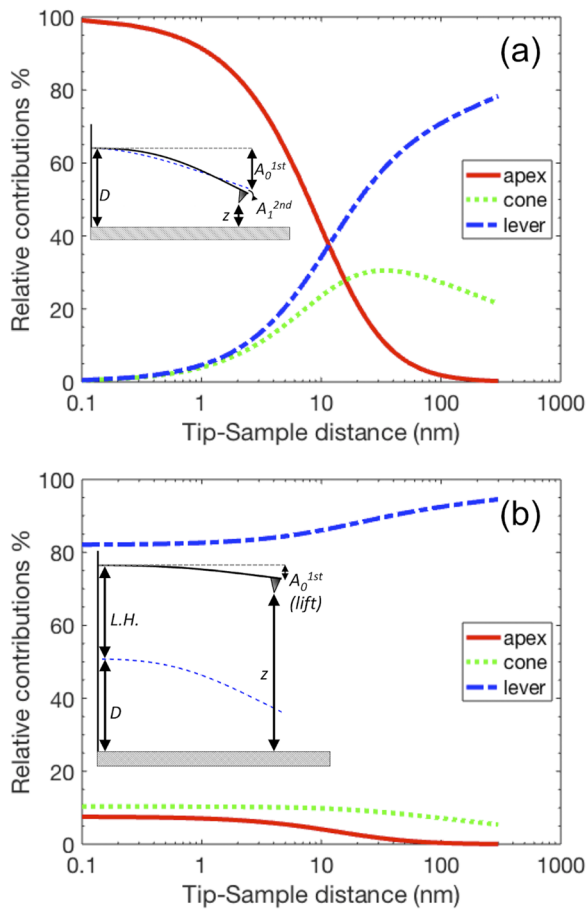


**FIG. 3.** Relative contributions of the capacitance first derivatives ( $\frac{\partial C}{\partial z}$ ) for the spherical tip apex, the cone, and the rectangular cantilever in both methods: (a) BM SS-EFM and (b) lift-mode KPFM with  $LH = 20$  nm. The drawings in the inset of each graph depict the shape of the cantilever and the overall distance between the tip and the sample in each mode.

spatial resolution obtained in this work fits with  $D_{area} = 28$  nm for  $a = 1.14$ . This is in very good agreement with the proposed analysis in Refs. 13 and 14.

In lift-mode KPFM, the distance between the tip and the sample is increased by the added lift height  $LH = 20$  nm. During the lift scan, the probe is oscillating at the first eigenmode of the cantilever's vibrations with an electrical driving signal. We note that the amplitude of oscillations in the lift scan  $A_0^{1st}$  is smaller than the amplitude of the mechanical oscillation  $A_0$ . The inset in Fig. 3(b) shows that the tip-sample distance could be expressed in this case as  $z = D + LH - (H + A_0^{1st})$ . The dashed blue line, plotted for visual guidance, represents the shape of the cantilever at its first eigenmode in the topography AM-AFM scan. Due to the increased separation distance in the lift-mode KPFM scan, the relative contributions shown in Fig. 3 indicate that the electrical force is dominated by the cantilever for the entire span of distances up to 300 nm and above. This explains the poor spatial resolution and the blurry contrast on the

contact potential images obtained in lift-mode KPFM [see Figs. 1(b) and 2(b)].

One of the questions that arise is about the possibility of reducing the lift height ( $LH$ ) even to negative values, which would mean bringing the cantilever to much smaller distances closer to the sample compared to that of the AM-AFM topography scan. Although, in principle, such a suggestion is feasible, it, however, has an important risk of damaging the tip by crashing it into the sample because of the absence of any distance feedback mechanism during the lift-mode scan. At closer separations, and in the absence of a distance control feedback, the interplay between electrostatic and van der Waals forces becomes important. Therefore, gradients of the total interaction force between the tip and sample in such a case could very likely overcome the stiffness of the cantilever (which is usually low to enhance the sensitivity of electrical force measurements) and lead to the intermittent or permanent crashing of the tip onto the surface. Nevertheless, several authors have reported the use of single scan KPFM schemes in which the choice of the mechanical and electrical driving frequencies is made such that the electrically driven oscillations match the frequency of the first eigenmode. These configurations, obviously, overcome the distance feedback problem by operating the AM-AFM and KPFM simultaneously much closer to the sample surface. However, our calculations (e.g., [supplementary material](#)) show that the bimodal shape of the cantilever, when the electrical vibrations are excited at the second eigenmode, enhances the relative contribution of the spherical tip apex at much larger distances between the tip and the sample. Thus, bimodal single scan KPFM methods are expected to have a higher spatial resolution. We note that this argument is only valid for amplitude modulation KPFM methods in which the probed signal corresponds to the electrostatic force  $F_{\omega_{el}}$  as it is the case of BM SS-EFM. However, frequency modulation KPFM methods, based on the detection of the electrostatic force gradient  $\frac{\partial F_{\omega_{el}}}{\partial z}$ , have higher spatial resolutions. Using the probe parameters in our experiments, we have estimated the relative capacitive contributions of the probe geometrical parts in the case of force gradient detection (e.g., [supplementary material](#)). We find, as an indication, that in force gradient modes, the contribution of the spherical apex dominates (larger than 45%) the electrostatic force at the tip-sample distance as high as 60 nm. This has been demonstrated experimentally in multiple works<sup>15,47,48</sup> showing that using force gradient detection in lift-mode KPFM still exhibits high spatial resolutions.

## B. Humidity effect on the electrical contrast

Reaching the 5 nm limit in spatial resolution using BM SS-EFM in humidity-reduced environment constitutes a step forward in imaging nanostructured materials allowing to capture their morphology and structure evolving *in situ* without relying on UHV heavy instrument. To comprehend the origin of the contrast and resolution enhancement, it is necessary to discuss the interaction of water molecules with graphene. It is well admitted that the wetting properties of graphene are strongly dependent on its surface-water interaction potential.<sup>49,50</sup> This is due to the water molecule dipoles responsible for altering the graphene surface potential and work of adhesion.<sup>51</sup> Indeed, Shafrin and Zisman<sup>52</sup> were the firsts to reveal that polar interactions strongly influence the wettability of metals,

which was later investigated in detail considering various geometric configurations of water dipoles with respect to the metal surface.<sup>49</sup> Recently, Giusca *et al.*<sup>53</sup> studied the affinity of graphene to water depending on the number of graphene layers. The authors studied the variations in the contact potential difference of epitaxial graphene on SiC-6H (0001), similar to our sample, by varying the environmental conditions between ambient, N<sub>2</sub> (RH < 10% to RH ~ 70%), and vacuum. Their results show that for ambient humidity 40%–50%, the work functions of 1LG and 2LG are almost equal (Fig. 4 in Ref. 53), while a large difference with 3LG is obtained at this ambient humidity level. The analysis of these results in Ref. 53 indicates that for a sample coverage of 1LG–2LG in ambient, the contact potential contrast is expected to be very small. If, however, the sample coverage is 1LG–3LG or 2LG–3LG, then the larger difference in their corresponding work functions would lead to higher contrast in contact potential difference. Since our experimental results in ambient, especially in lift-mode KPFM [Figs. 1(b) and 2(b)], show a blurry low contrast, it suggests that the scanned areas in our measurements show a 1LG–2LG coverage. This suggestion is supported by the fact that the results in Ref. 53 also show for the lowest RH% levels for N<sub>2</sub> < 10%, the difference between the work functions of 1LG and 2LG is large, while 2LG and 3LG have almost equal work functions. This means that under reduced humidity, the difference in the contact potential difference between 1LG and 2LG should be large leading to a sharper and brighter contrast. For 1LG–3LG or 2LG–3LG coverage, the difference in the contact potential difference under reduced humidity should be very small leading to a blurry contrast. Our BM SS-EFM results clearly show very sharp and highly resolved contrast for RH% ~ 2 ± 0.2%. It, thus, qualitatively implies that the highly resolved BM SS-EFM image in Fig. 2(c) clearly corresponds to the coverage of 2LG graphene layers (bright) grown over the SiC steps covered by 1LG (dark). This conclusion is in very good agreement with our previously reported measurements by x-ray photoemission electron microscopy (XPEEM) using the same sample, showing a major 1LG–2LG coverage of the SiC substrate.<sup>25,36</sup>

### C. Experimental boundaries of the BM SS-EFM method

#### 1. Effect of the electrostatic deflection

In the absence of a feedback loop to compensate the electrostatic forces in BM SS-EFM, it is important to evaluate the effect of these forces on the surface topography measured in AM-AFM. This will elucidate the contribution of crosstalk between channels. As described above, a compensation of the electrostatic forces in a closed-loop AM KPFM setup results in the application of a static bias voltage  $V_{dc} = V_{cpd}$ . Under ideal conditions, this would nullify the component of the force modulated electrically at  $\omega_{el}$ , as seen in Eq. (2), and reduces the value of the static component of the force in Eq. (1). In our BM SS-EFM method,  $V_{dc} = 0$ , which leaves the  $F_{\omega_{el}}$  component of the force uncompensated and  $F_{dc}$  unreduced. However, since the surface topography is measured in AM-AFM at the frequency of the mechanical oscillations  $\omega_m \neq \omega_{el}$ , the electrically modulated component  $F_{\omega_{el}}$  would have no effect on topography measurements as the detection lock-in amplifier filters out the corresponding signal. Nevertheless, the  $F_{dc}$  component of the electrical force would still induce a static deflection of the cantilever, which

changes the tip–sample separation distance. This change would alter the amplitude of the mechanical oscillations of the cantilever resulting in an artifact in topography measured in AM-AFM mode. We have carefully analyzed the possible limits of the static deflection caused by the unreduced  $F_{dc}$  and estimated their effect on the height topography measurement (e.g., supplementary material). We find that the possible height variation ( $\sim 1.4 \times 10^{-8}$  pm) falls far below the sensitivity limit of the vertical piezo sensor in the AFM system, which is about 30 pm.

Therefore, in our open-loop KPFM method, the presence of non-compensated electrostatic forces has no practical effect on the surface topography. This is true in the case of the sample with few layers of graphene coverage. It also extends to any other type of samples in which the variations in the contact potential differences are within comparable ranges.

#### 2. The stability of the imaging channels in BM SS-EFM

The AFM cantilever is driven simultaneously at its first two eigenmode frequencies  $f_0$  and  $f_1$ . The oscillating response is, therefore, subject to complicated dynamics between these modes. It has been shown that the excitation of the second eigenmode enhances the sensitivity of the AFM measurement to the interactions at longer tip–sample distances. The analytical investigation by Lozano and Garcia<sup>54</sup> demonstrates that, in the case of bimodal excitation, the amplitude of the first eigenmode is independent of the excitation scheme (e.g., whether it is mono-modal or bimodal). Nevertheless, the ratio between the amplitudes of the cantilever vibrations at the different eigenmodes plays an important role in defining the stability of such measurements. Results in Refs. 54 and 55 show that the amplitude of the first eigenmode can still be used for stable topography measurements in the AM-AFM mode (Tapping mode) as long as the free amplitude of vibrations at the second eigenmode is much lower than that of the first eigenmode oscillations. Other investigations have also pointed out the fact that the ratio of the energies, stored in the free vibrations of the cantilever at the different modes, also plays a crucial role in the stability of the oscillation dynamics.<sup>55,56</sup>

*a. Experimental observations.* The experimental conditions are another key element to achieve a stable simultaneous imaging of the surface topography and contact potential difference dependent properties of the sample in our BM SS-EFM method. In the following, the effects of experimental parameters on the imaging channels leading to stable measurements are determined; then, a more detailed analysis of the factors related to stable imaging in BM SS-EFM is performed to also draw the limits on the experimental parameters required to practically achieve simultaneous multi-modal driving of the cantilever to acquire surface topography and variations of the surface electrical properties.

As a first step, the effect of the external alternating bias voltage  $V_{ac}$  on the different imaging channels obtained during scanning was monitored, as shown in Fig. 4. Namely, we monitor the surface topography, amplitude, and phase of the cantilever's vibrations measured at the first eigenmode (noted by  $\omega_0 = 2\pi f_0$ ) during scanning. We simultaneously record the amplitude and the phase of the cantilever's electrically driven vibrations measured at  $\omega_1 = 2\pi f_1$ . We

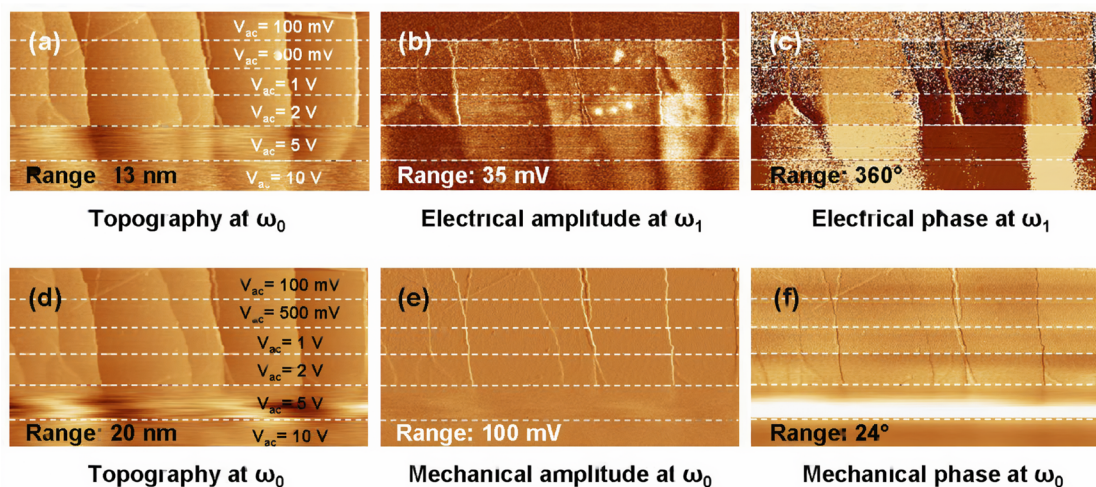


**FIG. 4.** (a) Surface topography recorded at  $\omega_0 = \frac{f_0}{2\pi}$ . (b) and (c) Amplitude  $A_1$  and phase  $\varphi_1$  signals of the electrically driven oscillations at  $\omega_1 = \frac{f_1}{2\pi}$ .  $V_{ac}$  was systematically changed during the scan between 0.1 V and 10 V. (d)–(f) Surface topography, amplitude  $A_0$ , and phase  $\varphi_0$  of the electrically driven oscillations at  $\omega_0$ . The effects of increasing the electrical drive  $V_{ac}$  are visually clear from the images and are discussed in the text.

recall that these latter channels were obtained through the measurement of the  $x_1$  and  $y_1$  outputs of the lock-in amplifier tuned at  $f_1$ .

During the scan, the external  $V_{ac}$  electrical drive amplitude has been changed between 0.1 V and 10 V. On the one hand, the imaging results in Figs. 4(d)–4(f) show that the amplitude  $A_0$  and phase  $\varphi_0$  of the cantilever's vibrations at the first eigenmode  $f_0$  remain unaltered by the simultaneous oscillations at the second eigenmode  $f_1$  for  $V_{ac} \leq 2$  V. On the other hand, the amplitude  $A_1$  of the electrical oscillations of the cantilever [Fig. 4(b)] presents a gradual increase in sensitivity to the potential dependent variations, related to graphene coverage on the sample, as the external electrical drive signal increases between  $V_{ac} = 0.1$  V and 2 V. At the lower limit of electrical excitations, the amplitude  $A_1$  shows a flat contrast. This indicates that the electrical oscillations at low driving signals ( $V_{ac} = 0.1$  V) are too small, and the sensitivity to electrical forces in this case is below the limits of the system detection. These observations correlate with the variations induced on the phase channel  $\varphi_1$ , as shown in Fig. 4(c). The very high noise level observed in the phase of the cantilever oscillations at  $f_1$  for the lowest limit of  $V_{ac} = 0.1$  V indicates that the electrical signal to noise ratio is low in this case. However, as  $V_{ac}$  increases, the noise on the phase channel  $\varphi_1$  decreases gradually to practically disappear for  $V_{ac} = 2$  V. This indicates that the sensitivity of the electrical oscillations at  $f_1$  to the contact potential surface dependency increases, leading to a stable imaging in BM SS-EFM. For higher driving voltages,  $V_{ac} > 2$  V, the contrast on the channel  $\varphi_1$  indicates important jumps in phase as well as smeared and noisy edges between potential dependent areas. Similar modifications can be also noticed on the contrast of the amplitude channel  $A_1$ . The changes observed on the channels of electrical oscillation at the second eigenmode  $f_1$  for high are directly correlated with a complete alteration of the AM-AFM topography measurement at the first eigenmode  $f_0$ . The contrast in Fig. 4(f) shows an important jump in the phase of

the mechanical vibrations at  $f_0$ , which suggests important changes in the imaging regimes in the AM-AFM mode. Nevertheless, for  $V_{ac} > 2$  V, the amplitude of mechanical oscillation at  $f_0$  is totally distorted, which appears in the loss of feedback during the topography scan [Fig. 4(d)].

All these observations suggest that the increase in the electrical oscillation amplitude at  $f_1$  (by increasing the  $V_{ac}$  driving signal) had led to a dynamical coupling between the eigenmode vibrations of the cantilever. For  $V_{ac} \leq 2$  V, the amplitude of mechanical vibrations  $A_0$  is stable as a feedback parameter for imaging surface topography in AM-AFM mode at  $f_0$ . For  $V_{ac} > 2$  V, the electrical oscillations at  $f_1$  coupled to those at  $f_0$  and the amplitude of the mechanical vibrations  $A_0$  is no longer stable leading to a loss of surface topography feedback at  $f_0$ . Although  $V_{ac} = 2$ , V is found to provide stable simultaneous imaging at both vibrational eigenmodes in our case, it is only specific to the experimental setup used in this work. We are, however, interested to draw a general understanding of the imaging stability conditions for our bimodal single-scan method. For this, we have investigated the relationship between the free amplitude of vibrations for both the first and second eigenmodes as suggested in Ref. 54 as well as the ratio of their respective free oscillations energies as modeled in Ref. 55.

*b. Ratios of amplitudes and stored energies. Free amplitudes of vibrations.* We investigated the free amplitudes of cantilever vibrations at the first and second modes as well as the energies stored in the oscillations for each mode, following the suggested theoretical work in Refs. 54 and 55. All vibration amplitudes are determined away from the sample surface and are referred to (with an upper index “0”) as free vibrational amplitudes. Thus,  $A_0^{(0)}$  and  $A_1^{(0)}$  represent the amplitudes of free oscillations at the first ( $f_0$ ) and second ( $f_1$ ) eigenmode frequencies, respectively. The experimental procedure, used in determining these amplitudes,



consisted of the following steps. First, the probe is withdrawn several micrometers away from the surface to ensure no interaction with the AFM tip. Then, the cantilever is driven to oscillations mechanically by the mean of the dither piezo. The frequency of the driving signal is fine-tuned so that the vibrational response of the cantilever matches with the resonance at the first eigenmode frequency  $f_0 = 65$  kHz. The rms amplitude reading on the AFM system is set in this case to  $A_0^{rms} = 2$  V, which corresponds to an amplitude of oscillations calibrated at  $A_0^{(0)} \cong 50$  nm. In a second step, the mechanical drive through the dither piezo is switched off. The external electric driving signal  $V_{ac} \sin(\omega_e t)$  is then directly applied to the probe. The vibrational response of the cantilever is tuned such that  $\omega_{el} = \omega_1 = 2\pi f_1$ , where  $f_1 = 392$  kHz is the frequency of the second eigenmode. A linear relationship was found between the magnitude of the external voltage  $V_{ac}$  and the rms amplitude reading of the electrically driven cantilever's vibrations such that  $A_1^{rms}(\text{volts}) = V_{ac}/3$  (e.g., [supplementary material](#)). The sensitivity of the cantilever deflection at the second eigenmode is determined using amplitude vs distance curves (not shown here) in order to calibrate the oscillation amplitude  $A_1^{(0)}$  in nanometers. The cantilever stiffness  $k_1$  at the second eigenmode is derived using the power law  $k_n = k_0(f_n/f_0)^2$  and is found around  $k_1 = 109.11 \text{ N m}^{-1}$  for the cantilever used in our experiments. [Table I](#) shows all the values of the free amplitudes for both vibrational modes. We recorded the cantilever's deflection during scanning when the probe is driven at  $f_0$  and  $f_1$ , simultaneously, as shown in [Fig. 5](#). For small values of the external electrical driving signal  $V_{ac} \leq 2$  V, the total deflection of the cantilever corresponds to a linear superposition of the two oscillations at the first and second eigenmode frequencies. The electrically driven cantilever's vibration at  $f_1$  can be considered under these conditions as a small perturbation to the oscillation of the cantilever mechanically driven at  $f_0$ . This preserves the dynamics of the system as governed by the envelope oscillation at the first eigenmode. This correlates with the observations made above on the imaging channels in which the amplitude of vibrations at  $f_0$  is stable and can be used for AM-AFM topography imaging. These considerations are supported by the evaluated ratio of the free oscillation amplitudes for the two eigenmodes  $A_1^{(0)}/A_0^{(0)}$

shown in [Table I](#). For low electrical drive at  $f_1$ , the free oscillation amplitude  $A_1^{(0)}$  is a very small fraction of  $A_0^{(0)}$ . At  $V_{ac} = 2$  V, the ratio  $A_1^{(0)}/A_0^{(0)}$  reaches the value 0.13, which is in very good agreement with the theoretical predictions in [Ref. 54](#), which suggested for a stable use of the oscillations at the first eigenmode for AM-AFM topography feedback. As  $V_{ac}$  increases between 0.1 V and 2 V, the intensity of the perturbation increases, which has a positive effect on improving the sensitivity of the cantilever oscillations at  $f_1$  to the electrostatic forces as observed on the imaging channels  $A_1$  and  $\varphi_1$  in [Fig. 4](#).

Nevertheless, the dynamics of the cantilever's deflection become totally distorted when  $V_{ac}$  is increased above 2 V. [Figure 5](#) shows that for high electrical driving signals,  $V_{ac} = 5$  V and  $V_{ac} = 10$  V, the electrical oscillations at  $f_1$  can no longer be considered as a small perturbation to the mechanical oscillations. In fact, the envelope signal at  $f_0$  is completely lost in these cases, and the cantilever's deflection indicates strongly coupled dynamics between the two modes of vibration. This clearly results in  $A_0$  being no longer stable to be used as a feedback signal for topography measurements in AM-AFM as previously demonstrated on the imaging channels in [Fig. 4](#). Interestingly, however, [Table I](#) shows that the ratio of the free oscillation amplitudes of the two modes,  $A_1^{(0)}/A_0^{(0)}$ , remains smaller than unity even for the largest values of the electrical driving signal. This means that in all the cases presented here, the amplitude of free electrical oscillation at  $f_1$  remained smaller than that of the free mechanical oscillations at  $f_0$ . Therefore, the ratio of the free oscillation amplitudes of the two modes,  $f_0$  and  $f_1$ , does not constitute a differentiation factor to identify general stable imaging conditions in the BM SS-EFM method. For this, we have investigated the ratio of the energies stored in the oscillations at each mode in order to analyze its correlation with the stable simultaneous imaging in AM-AFM topography measurement and BM SS-EFM.

*Energy stored in the vibrational eigenmodes.* The energy stored in each vibrational mode was evaluated by calculating the average value of the Hamiltonian  $H = T + U$  for the vibrating probe integrated over one period of oscillations. By considering the

**TABLE I.** Experimental free amplitude of vibrations at both eigenmodes as rms and calibrated values. Energies stored in the free vibrations for each vibrational eigenmode as estimated from  $\langle H \rangle_n^{(0)}$ . Ratios of the second to the first eigenmode for the free amplitudes of vibrations and energies stored in free oscillations.

$A_0^{(0)}$ (nm)	$E_0^{(0)}$ (J)	$V_{ac}$ (V)	$A_1^{rms}$ (V)	$A_1^{(0)}$ (nm)	$E_1^{(0)}$ (J)	$A_1^{(0)}/A_0^{(0)}$	$E_1^{(0)}/E_0^{(0)}$
First eigenmode		Second eigenmode					
$f_0 = 65$ kHz		$f_1 = 392$ kHz					
$k_0 = 3 \text{ N m}^{-1}$		$k_1 = 109 \text{ N m}^{-1}$					
50	11 781	0.1	0.033	0.32	17.55	0.0064	0.0015
		0.5	0.166	1.6	438.76	0.032	0.0372
		1	0.333	3.2	1 755.03	0.064	0.15
		2	0.666	6.4	7 020.13	0.13	0.6
		5	1.666	16	43 875.8	0.32	3.72
		10	3.333	32	175 503	0.64	14.9



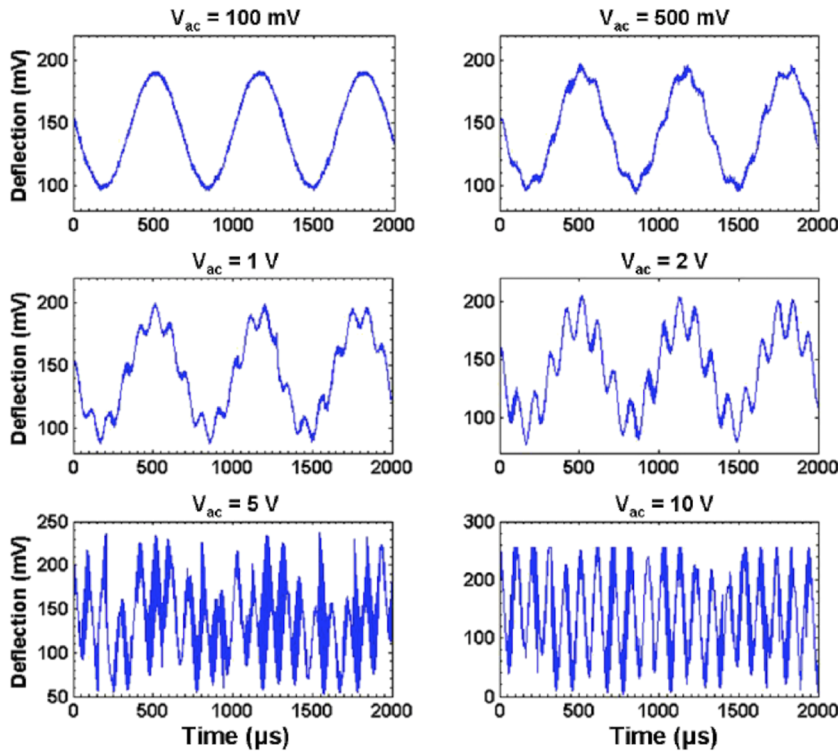


**FIG. 5.** The cantilever deflection signal monitored during the scan for different values of the external electrical driving signal  $V_{ac}$ . The cantilever is simultaneously driven mechanically at  $f_0$  and electrically at  $f_1$ .

free amplitude of vibrations with no interaction forces with the surface, the Hamiltonian for each mode is found as  $\langle H \rangle_n^{(0)} = \frac{\pi}{2} \frac{k_n (A_n^{(0)})^2}{\omega_n^2} (1 + \omega_n^2)$ , with  $n = 0, 1$  corresponding to the first and second eigenmodes, respectively. Table I shows that, for  $0.1 \text{ V} \leq V_{ac} \leq 2 \text{ V}$ , the ratio of the energies stored in the free oscillations at the first and second eigenmodes remains smaller than the unity and was found in the range  $0.0015 \leq E_1^{(0)}/E_0^{(0)} \leq 0.6$ . For larger  $V_{ac}$  values, this ratio is  $E_1^{(0)}/E_0^{(0)} > 1$ . In correlation with the arguments put forward in the previous paragraphs, the electrical oscillations act as a perturbation to the mechanical vibrations as long as the total energy stored in the cantilever's free vibrations at the second eigenmode  $f_1$  is much smaller than that stored in the free mechanical vibrations at  $f_0$ . This also indicates that the dynamical coupling between the two modes occurs when the experimental parameters are set such that the energy stored in the free electrical oscillations at the second eigenmode exceeds the energy stored in the free mechanical oscillations at the first eigenmode. In this latter case, the dynamics of the cantilever are no longer dominated by the oscillations at  $f_0$  as an envelope and the linear superposition of the two modes no longer holds.

It is clear that the energy stored in the second eigenmode frequency of the cantilever's free vibrations plays a crucial role in defining the experimental conditions for a stable imaging in BM SS-EFM. The choice of the electrical driving signal  $V_{aca}$  should, therefore, be made according to satisfy the condition  $E_1^{(0)}/E_0^{(0)} < 1$ . This could be easily found by the estimation of the Hamiltonian, as expressed here, using the experimental values of cantilever's spring constant

$k_n$ , the eigenmode frequency  $f_n$ , and the calibrated free amplitude of oscillations  $A_n^{(0)}$ .

Figures 6(a) and 6(b) show the variations of  $A_1^{(0)}/A_0^{(0)}$  and  $E_1^{(0)}/E_0^{(0)}$  as a function of  $V_{ac}$ . The dashed lines indicate the critical value of the electrical driving signal suitable for stable imaging in our case. Similar plots could be used for any other setup of BM SS-EFM to delimit the selection criteria of experimental values for stable imaging. The ratios of free oscillation amplitudes and stored energies offer sufficient information on the experimental configuration stability in bimodal AFM setups. Nevertheless, in KPFM-related methods, the selection of  $V_{ac}$  is also strongly related to the sensitivity of the electrical measurements, namely, the minimum measurable contact potential difference (CPD).

*c. Sensitivity in BM SS-EFM.* We have estimated the sensitivity of our measurements to the local variations in potential dependent properties of the sample by calculating the minimal measurable value of the CPD and considering only the thermal noise of the cantilever. The smallest measurable value of CPD corresponds to the smallest measurable electric force. This is derived from a signal to noise ratio  $S/R = \frac{f}{\sqrt{4k_B T c B}} = 1$ , where  $f$  is the electrical force,  $k_B$  is the Boltzmann constant,  $T$  is the temperature in Kelvin,  $B$  being the detection bandwidth in Hz, and  $c = k_0/Q\omega_0$  is the friction coefficient. By setting  $V_{dc} = 0$ , the minimal CPD value ( $V_{cpd}^{min}$ ) is given by

$$V_{cpd}^{min} = \frac{1}{V_{ac}} \sqrt{\frac{4k_B k_0 T B}{Q\omega_0}} \left( \frac{\partial C}{\partial z} \right)^{-1}.$$

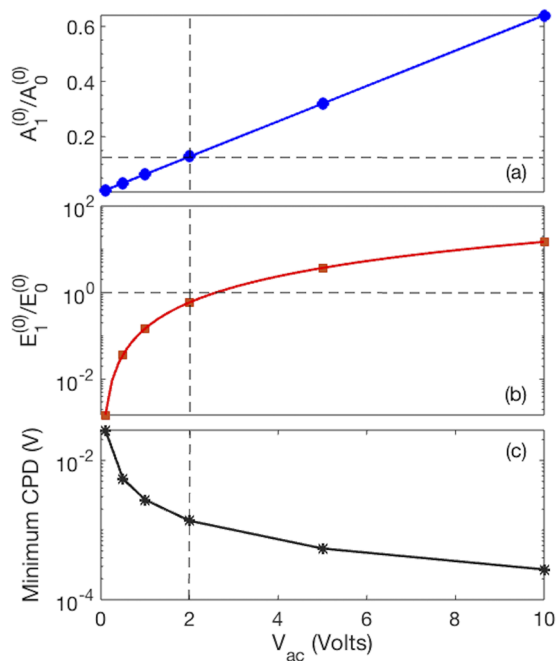


**FIG. 6.** Plots of the calculated ratios of (a) the free vibration amplitudes at the first two eigenmodes as a function of the electrical driving signal  $V_{ac}$ ; (b) the ratio of the energies stored in the cantilever's free oscillations at the first two eigenmodes. (c) Calculated values of the minimum CPD for different  $V_{ac}$ . The dashed lines indicate the case of  $V_{ac} = 2$  V used in the current experimental measurements.

This relation holds generally for any KPFM scheme as the expression of the electrical force remains the same for all KPFM variant methods. In addition to the intrinsic properties of the selected cantilever (not discussed in this work), the sensitivity has various dependencies on different experimental parameters of the measurement configuration. A reduced bandwidth would result in a higher sensitivity as  $V_{cpd}^{min}$  becomes smaller. However, this leads to lower scanning speeds, which is not necessarily a desirable condition. Nonetheless, increasing the electrical driving signal  $V_{ac}$  results in a better sensitivity to the potential dependent properties of the sample, as shown in Fig. 6(c). We calculated the minimal CPD values for different  $V_{ac}$  considering a tip to sample mean separation distance  $d = 30$  nm. For  $V_{ac} = 2$  V, the minimum measurable CPD value in our case was found to be around 1.3 mV.

It is worth noting that in KPFM measurements, the sensitivity increases as the tip to sample distance increases. This could be understood by the fact that at higher distances from the surface, the larger components of the probe (cone and cantilever) start to have more predominant contribution to the capacitance. Therefore, more electrical signals could be picked up by the probe at larger distances, which increases the sensitivity of the measurement. This, however, has the drawback of decreasing the spatial resolution and the accuracy of the measured values of contact potential difference.<sup>12,14,36</sup>

## VI. CONCLUSION

In this work, the capability of BM SS-EFM was successfully demonstrated to provide qualitative imaging directly proportional to the local CPD variations, at particularly high resolution in ambient temperature and humidity-reduced environment down to 5 nm, at the same scanning rates as AM-AFM mode. Our analysis showed that the stability of the BM SS-EFM method relies essentially on the energy stored in the second eigenmode frequency of the cantilever vibrations. A ratio of  $E_1^{(0)}/E_0^{(0)} < 1$  is an experimental condition that has to be satisfied for stable bimodal imaging. We believe that the ratio of free amplitudes of vibrations at the two eigenmodes is important but not specific. We suggest that a ratio of  $A_1^{(0)}/A_0^{(0)} \sim 0.1 - 0.2$  would be naturally satisfied, if the ratio of stored energies as mentioned above is set smaller than unity. The sensitivity of the electrical measurement will result from the choices made of the electrical drive  $V_{ac}$  to satisfy the previously mentioned conditions. However, for better sensitivities, a larger tip-sample distance could be adopted on the detriment of lowering the spatial resolution. It is also possible to make use of different cantilevers with more suited properties to match a desired threshold of minimum measurable contact potential difference values.

We also showed in this work that BM SS-EFM provides an interesting tool to investigate low-dimensional materials at very high resolution under accessible conditions. This method benefits from several factors, which make it an attractive asset to material science community to capture nanoscale features ascribed to the physical properties of materials. The BM SS-EFM method is easy to implement on any commercial AFM system. It does not use a Kelvin feedback system, which avoids instrumental artifacts and restricted scanning speeds due to the bandwidth of the controller. This makes BM SS-EFM very attractive for the implementation on fast scanning AFM systems, which would provide means to qualitatively monitor the electrostatic properties of the surface on the fly at very high resolution. A further development could lead to a quantitative imaging of the contact potential difference. In fact, with the use of an additional lock-in amplifier, set to the double ( $2\omega_{el}$ ) of the electrical modulation frequency, one could be able to acquire the corresponding amplitude of the signal  $A_{2\omega_{el}}$  from Eq. (3). The contact potential maps in BM SS-EFM could then be obtained by computing the ratio of the signals  $A_{\omega_e}/A_{2\omega_e}$  such that (for  $V_{dc} = 0$ )

$$V_{cpd} = \frac{V_{ac}}{4} \cdot \frac{A_{\omega_e}}{A_{2\omega_e}}.$$

We note that such a signal manipulation is currently accessible and could be made in real scanning time, on most new advanced AFM systems. Quantitative  $V_{cpd}$  could thus be obtained during scanning without the need for additional signal post-processing. These features are not accessible on the system that we have used in this experimental work. Finally, we point out to the fact that using an additional lock-in amplifier tuned at the double of the electrical frequency ( $2\omega_e$ ) allows the direct measurement of the variations in the first gradient of the tip-sample capacitance related to the variation in the dielectric properties of the sample.

## SUPPLEMENTARY MATERIAL

See the [supplementary material](#) for polarization sign of the DC bias voltage, experimental setup of the BM SS-EFM method, electrical driving signal amplitudes, contribution of the static component of the force on surface topography, and capacitive contributions in single scan EFM methods using bimodal shape vs first eigenmode shape—BM SS-EFM vs force gradient sensitive detection modes.

## AUTHORS' CONTRIBUTIONS

K.K. designed the experiments, conducted measurements, collected and analyzed data, and wrote the manuscript. A.N. and M.J. participated in result interpretation and writing of the manuscript. D.M. and N.C. supervised the whole experimental work.

## ACKNOWLEDGMENTS

This work was funded by the commissariat à l'énergie atomique (CEA) in the framework of a Ph.D. project. The authors thank A. Chabli and G. Feuillet for the fruitful discussions and support, O. Renault for the help in comparing results by photoemission electron microscopy, and F. El Omar for his support at the LPM, EDST.

The authors declare no conflicts of interest.

## DATA AVAILABILITY

The data that support the findings of this study are available from the corresponding author upon reasonable request.

## REFERENCES

- 1 K. S. Novoselov, "Nobel lecture: Graphene: Materials in the Flatland," *Rev. Mod. Phys.* **83**, 837–849 (2011).
- 2 P. Sutter, "Epitaxial graphene: How silicon leaves the scene," *Nat. Mater.* **8**, 171–172 (2009).
- 3 K. S. Novoselov, D. Jiang, F. Schedin, T. J. Booth, V. V. Khotkevich, S. V. Morozov, and A. K. Geim, "Two-dimensional atomic crystals," *Proc. Natl. Acad. Sci. U. S. A.* **102**, 10451–10453 (2005).
- 4 R. Mas-Ballesté, C. Gómez-Navarro, J. Gómez-Herrero, and F. Zamora, "2D materials: To graphene and beyond," *Nanoscale* **3**, 20–30 (2011).
- 5 S. Das, J. A. Robinson, M. Dubey, H. Terrones, and M. Terrones, "Beyond graphene: Progress in novel two-dimensional materials and van der Waals solids," *Annu. Rev. Mater. Res.* **45**, 1–27 (2015).
- 6 M. Saint Jean, S. Hudlet, C. Guthmann, and J. Berger, "Van der Waals and capacitive forces in atomic force microscopies," *J. Appl. Phys.* **86**, 5245–5248 (1999).
- 7 K. Kaja, N. Chevalier, D. Mariolle, F. Bertin, G. Feuillet, and A. Chabli, "Effects of experimental parameters on the work function measurement: A Kelvin force microscopy study," *AIP Conf. Proc.* **1173**, 224–228 (2009).
- 8 D. Ziegler, "Techniques to quantify local electric potentials and eliminate electrostatic artifacts in atomic force microscopy," Ph.D. thesis, ETH Zurich, 2009.
- 9 S. Hudlet, M. Saint Jean, C. Guthmann, and J. Berger, "Evaluation of the capacitive force between an atomic force microscopy tip and a metallic surface," *Eur. Phys. J. B* **2**, 5–10 (1998).
- 10 P. Girard, "Electrostatic force microscopy: Principles and some applications to semiconductors," *Nanotechnology* **12**, 485–490 (2001).
- 11 H. O. Jacobs, H. F. Knapp, S. Müller, and A. Stemmer, "Surface potential mapping: A qualitative material contrast in SPM," *Ultramicroscopy* **69**, 39–49 (1997).
- 12 H. O. Jacobs, P. Leuchtmann, O. J. Homan, and A. Stemmer, "Resolution and contrast in Kelvin probe force microscopy," *J. Appl. Phys.* **84**, 1168–1173 (1998).
- 13 P. Girard and A. N. Titkov, "Electrostatic force and force gradient microscopy: Principles, points of interest and application to characterisation of semiconductor materials and devices," in *Applied Scanning Probe Methods II. NanoScience and Technology*, edited by B. Bhushan and H. Fuchs (Springer, Berlin, Heidelberg, 2006), pp. 283–320.
- 14 M. Dunaevskiy, P. Alekseev, P. Girard, A. Lashkul, E. Lahderanta, and A. Titkov, "Analysis of the lateral resolution of electrostatic force gradient microscopy," *J. Appl. Phys.* **112**, 064112 (2012).
- 15 D. Ziegler and A. Stemmer, "Force gradient sensitive detection in lift-mode Kelvin probe force microscopy," *Nanotechnology* **22**, 075501 (2011).
- 16 A. Gil, J. Colchero, J. Gómez-Herrero, and A. M. Baró, "Electrostatic force gradient signal: Resolution enhancement in electrostatic force microscopy and improved Kelvin probe microscopy," *Nanotechnology* **14**, 332–340 (2003).
- 17 U. Zerweck, C. Loppacher, T. Otto, S. Grafström, and L. M. Eng, "Accuracy and resolution limits of Kelvin probe force microscopy," *Phys. Rev. B* **71**, 125424 (2005).
- 18 R. A. Oliver, "Advances in AFM for the electrical characterization of semiconductors," *Rep. Prog. Phys.* **71**, 076501 (2008).
- 19 A. K. Henning, T. Hochwitz, J. Slinkman, J. Never, S. Hoffmann, P. Kaszuba, and C. Daghljan, "Two-dimensional surface dopant profiling in silicon using scanning Kelvin probe microscopy," *J. Appl. Phys.* **77**, 1888–1896 (1995).
- 20 J. M. R. Weaver, "High resolution atomic force microscopy potentiometry," *J. Vac. Sci. Technol.*, **B 9**, 1559 (1991).
- 21 A. Kikukawa, S. Hosaka, and R. Imura, "Silicon pn junction imaging and characterizations using sensitivity enhanced Kelvin probe force microscopy," *Appl. Phys. Lett.* **66**, 3510–3512 (1995).
- 22 C. Örnek and D. L. Engelberg, "An experimental investigation into strain and stress partitioning of duplex stainless steel using digital image correlation, x-ray diffraction and scanning Kelvin probe force microscopy," *J. Strain Anal. Eng. Des.* **51**, 207–219 (2016).
- 23 C. Örnek and D. L. Engelberg, "SKPFM measured Volta potential correlated with strain localisation in microstructure to understand corrosion susceptibility of cold-rolled grade 2205 duplex stainless steel," *Corros. Sci.* **99**, 164–171 (2015).
- 24 T. Filleter, K. V. Emtsev, T. Seyller, and R. Bennewitz, "Local work function measurements of epitaxial graphene," *Appl. Phys. Lett.* **93**, 133117 (2008).
- 25 O. Renault, A. M. Pascon, H. Rotella, K. Kaja, C. Mathieu, J. E. Rault, P. Blaise, T. Poiroux, N. Barrett, and L. R. C. Fonseca, "Charge spill-out and work function of few-layer graphene on SiC(0001)," *J. Phys. D: Appl. Phys.* **47**, 295303 (2014).
- 26 J. Lü, E. Delamar, L. Eng, R. Bennewitz, E. Meyer, and H.-J. Güntherodt, "Kelvin probe force microscopy on surfaces: Investigation of the surface potential of self-assembled monolayers on gold," *Langmuir* **15**, 8184–8188 (1999).
- 27 D. Ziegler, P. Gava, J. Güttinger, F. Molitor, L. Wirtz, M. Lazzeri, A. M. Saitta, A. Stemmer, F. Mauri, and C. Stampfer, "Variations in the work function of doped single- and few-layer graphene assessed by Kelvin probe force microscopy and density functional theory," *Phys. Rev. B* **83**, 235434 (2011).
- 28 N. J. Lee, J. W. Yoo, Y. J. Choi, C. J. Kang, D. Y. Jeon, D. C. Kim, S. Seo, and H. J. Chung, "The interlayer screening effect of graphene sheets investigated by Kelvin probe force microscopy," *Appl. Phys. Lett.* **95**, 222107 (2009).
- 29 Y. Almadori, D. Moerman, J. L. Martinez, P. Leclère, and B. Grévin, "Multimodal noncontact atomic force microscopy and Kelvin probe force microscopy investigations of organolead tribromide perovskite single crystals," *Beilstein J. Nanotechnol.* **9**, 1695–1704 (2018).
- 30 T. Glatzel, H. Hoppe, N. S. Sariciftci, M. C. Lux-Steiner, and M. Komiyama, "Kelvin probe force microscopy study of conjugated polymer/fullerene organic solar cells Japanese," *J. Appl. Phys.* **44**, 5370–5373 (2005).
- 31 V. Palermo, M. Palma, and P. Samori, "Electronic characterization of organic thin films by Kelvin probe force microscopy," *Adv. Mater.* **18**, 145–164 (2006).
- 32 A. K. Sinensky and A. M. Belcher, "Label-free and high-resolution protein/DNA nanoarray analysis using Kelvin probe force microscopy," *Nat. Nanotechnol.* **2**, 653–659 (2007).
- 33 H. Xie, H. Zhang, D. Hussain, X. Meng, J. Song, and L. Sun, "Multiparametric Kelvin probe force microscopy for the simultaneous mapping of surface potential and nanomechanical properties," *Langmuir* **33**, 2725–2733 (2017).

- <sup>34</sup>D. El Khoury, "Towards the use of electrostatic force microscopy to study interphases in nanodielectric materials," Ph.D. thesis, Université de Montpellier, France, 2018.
- <sup>35</sup>L. Collins, J. I. Kilpatrick, S. A. L. Weber, A. Tselev, I. V. Vlassioux, I. N. Ivanov, S. Jesse, S. V. Kalinin, and B. J. Rodriguez, "Open loop Kelvin probe force microscopy with single and multi-frequency excitation," *Nanotechnology* **24**, 475702 (2013).
- <sup>36</sup>K. Kaja, "Development of nanoprobe techniques for work function assessment and application to material for microelectronics," Ph.D. thesis, University Grenoble Alpes (2010).
- <sup>37</sup>D. Rouchon, L. Becerra, O. Renault, K. Kaja, D. Mariolle, and N. Chevalier, "Raman spectra and imaging of graphene layers grown by SiC sublimation," *AIP Conf. Proc.* **1267**, 445–446 (2010).
- <sup>38</sup>H. Hibino, H. Kageshima, M. Kotsugi, F. Maeda, F. Z. Guo, and Y. Watanabe, "Dependence of electronic properties of epitaxial few-layer graphene on the number of layers investigated by photoelectron emission microscopy," *Phys. Rev. B* **79**, 125437 (2009).
- <sup>39</sup>W. E. S. Unger, M. Senoner, T. Wirth, S. Bütetfisch, and I. Busch, "Lateral resolution of imaging surface-analytical instruments as SIMS, AES and XPS: Application of the BAM-L200 certified reference material and related ISO standards," *J. Surf. Anal.* **24**, 123–128 (2017).
- <sup>40</sup>M. Senoner, A. Maaßdorf, H. Roock, W. Österle, M. Malcher, M. Schmidt, F. Kollmer, D. Paul, V.-D. Hodoroaba, S. Rades, and W. E. S. Unger, "Lateral resolution of nanoscaled images delivered by surface-analytical instruments: Application of the BAM-L200 certified reference material and related ISO standards," *Anal. Bioanal. Chem.* **407**, 3211–3217 (2015).
- <sup>41</sup>M. Senoner, T. Wirth, and W. E. S. Unger, "Imaging surface analysis: Lateral resolution and its relation to contrast and noise," *J. Anal. At. Spectrom.* **25**, 1440–1452 (2010).
- <sup>42</sup>H. N. McMurray and G. Williams, "Probe diameter and probe-specimen distance dependence in the lateral resolution of a scanning Kelvin probe," *J. Appl. Phys.* **91**, 1673–1679 (2002).
- <sup>43</sup>X. D. Ding, J. An, J. B. Xu, C. Li, and R. Y. Zeng, "Improving lateral resolution of electrostatic force microscopy by multifrequency method under ambient conditions," *Appl. Phys. Lett.* **94**, 223109 (2009).
- <sup>44</sup>C. Sommerhalter, T. Glatzel, T. W. Matthes, A. Jäger-Waldau, and M. C. Lux-Steiner, "Kelvin probe force microscopy in ultra high vacuum using amplitude modulation detection of the electrostatic forces," *Appl. Surf. Sci.* **157**, 263–268 (2000).
- <sup>45</sup>N. Gaillard, "Etude des propriétés morphologiques, électriques et chimiques de l'interface métal/isolant et de leur impact sur les performances de la capacité TiN/Ta<sub>2</sub>O<sub>5</sub>/TiN," Ph.D. thesis, University Grenoble Alpes (2007).
- <sup>46</sup>H. Sugimura, Y. Ishida, K. Hayashi, O. Takai, and N. Nakagiri, "Potential shielding by the surface water layer in Kelvin probe force microscopy," *Appl. Phys. Lett.* **80**, 1459–1461 (2002).
- <sup>47</sup>L. Portes, M. Ramonda, R. Arinero, and P. Girard, "New method for electrostatic force gradient microscopy observations and Kelvin measurements under vacuum," *Ultramicroscopy* **107**, 1027–1032 (2007).
- <sup>48</sup>L. Portes, P. Girard, R. Arinero, and M. Ramonda, "Force gradient detection under vacuum on the basis of a double pass method," *Rev. Sci. Instrum.* **77**, 096101 (2006).
- <sup>49</sup>H. J. Lee, A. C. Jamison, and T. R. Lee, "Surface dipoles: A growing body of evidence supports their impact and importance," *Acc. Chem. Res.* **48**, 3007–3015 (2015).
- <sup>50</sup>Z. Li, Y. Wang, A. Kozbial, G. Shenoy, F. Zhou, R. McGinley, P. Ireland, B. Morganstein, A. Kunkel, S. P. Surwade, L. Li, and H. Liu, "Effect of airborne contaminants on the wettability of supported graphene and graphite," *Nat. Mater.* **12**, 925–931 (2013).
- <sup>51</sup>C. Melios, C. E. Giusca, V. Panchal, and O. Kazakova, "Water on graphene: Review of recent progress," *2D Mater.* **5**, 022001 (2018).
- <sup>52</sup>E. G. Shafrin and W. A. Zisman, "The adsorption on platinum and wettability of monolayers of terminally fluorinated octadecyl derivatives," *J. Phys. Chem.* **61**, 1046–1053 (1957).
- <sup>53</sup>C. E. Giusca, V. Panchal, M. Munz, V. D. Wheeler, L. O. Nyakiti, R. L. Myers-Ward, D. K. Gaskill, and O. Kazakova, "Water affinity to epitaxial graphene: The impact of layer thickness," *Adv. Mater. Interfaces* **2**, 1500252 (2015).
- <sup>54</sup>J. R. Lozano and R. Garcia, "Theory of multifrequency atomic force microscopy," *Phys. Rev. Lett.* **100**, 076102 (2008).
- <sup>55</sup>R. W. Stark, "Dynamics of repulsive dual-frequency atomic force microscopy," *Appl. Phys. Lett.* **94**, 063109 (2009).
- <sup>56</sup>D. Kiracofe and A. Raman, "On eigenmodes, stiffness, and sensitivity of atomic force microscope cantilevers in air versus liquids," *J. Appl. Phys.* **107**, 033506 (2010).